Proceedings of the IASS 2024 Symposium
Redefining the Art of Structural Design
August 26-30, 2024, Zurich Switzerland
Philippe Block, Giulia Boller, Catherine DeWolf,
Jacqueline Pauli, Walter Kaufmann (eds.)

Design of Concrete Plates and Shells: A Solved Problem?

Vera BALMER*, Karel THOMA, Walter KAUFMANN

*ETH Zürich, Switzerland
Stefano-Franscini Platz 5, 8093 Zürich
vera.balmer@ibk.baug.ethz.ch

Abstract

Reinforced concrete is the most widely used material for plates and shells. While one might thus assume that their dimensioning is a long-solved problem, many questions remain open. The design of shells often aims at minimising bending moments using appropriate geometries. However, pure membrane action cannot be achieved under varying loads, as concrete shells are too stiff to adapt their form. On the other hand, while bending governs the behaviour of floor slabs, compressive or tensile membrane forces inevitably develop due to cracking or large deflections, respectively. Moreover, the principal directions of internal actions vary depending on the loading. Concrete plates and shells are thus typically subjected to eight independent stress resultants. If ductile behaviour is ensured, a simple sandwich model approach based on plasticity theory is sufficient to design the reinforcement and check for structural safety. However, this requires redistribution of internal forces and thus cannot be used to verify e.g. the fatigue resistance or serviceability where the actual load-deformation behaviour must be considered. No simplified design methods enable such analyses, not even for linear elastic behaviour. On the other hand, nonlinear layered shell element models, developed for this purpose decades ago, are established but computationally intensive and are considered an expert tool. Covering the related uncertainties by overdesigning new – or potentially unnecessarily strengthening existing – structures is no longer viable in light of the need to reduce the carbon footprint of construction. Instead, the mechanical behaviour must be known and understood precisely. The paper therefore outlines a case study comparing analytical and numerical approaches for the fundamental case of pure twisting moments, either neglecting or accounting for membrane action, including a new theoretical solution for the latter case. Finally, the study formulates a baseline of knowledge gaps about the behaviour of concrete plates and shells and how these should be tackled in future research.

Keywords: concrete plates and shells, reinforcement design, sandwich model, layered shell element, experimental testing

1. Introduction

Reinforced concrete (RC) is the most widely used construction material for plates and shells. These elements are the fundamental components of larger structures such as bridges, floor slabs or other infrastructure. Thus, when analysing the structural safety or serviceability of RC structures, it is inherently crucial to understand their mechanical behaviour on a shell or plate element level. Particularly in light of the high carbon footprint of the construction industry, the material behaviour must be known and understood more precisely than ever to build structurally efficient and material-saving structures.

Plates, as well as shells, are typically loaded perpendicularly to their mid-plane, but differ by their geometry and load-bearing behaviour. Plates (often referred to as slabs) are a type of plane structure carrying loads perpendicular to their mid-plane and predominantly subjected to bending and twisting moments (m_x, m_y, m_{xy}) and transverse shear forces (v_x, v_y) [1]. Shells, on the other hand, may be curved and are thus – even if only loaded perpendicularly to their mid-plane – additionally subjected to membrane forces (n_x, n_y, n_{xy}), leading to a more complex mechanical behaviour with eight stress

resultants (bending moments $m_x,\ m_y,\ m_{xy}$, transverse shear forces v_x, v_y and membrane normal and shear forces n_x, n_y, n_{xy}). On the other hand, membrane forces also develop in non-curved RC plates, e.g. due to cracking or combined load-carrying functions, such as in bridge decks transferring traffic loads locally (bending action) while at the same time serving as flange of a girder (membrane action). Hence, elements of plates are generally subjected to the same eight stress resultants as shell elements, and the mechanical behaviour on the element level can be analysed with the same models; they are thus referred to as *shell elements* in the following. Note that this study focuses on compressive membrane action (CMA) in RC plates, neglecting tensile membrane forces as well as geometrical nonlinearities.

Similar to a RC beam in bending, the response of RC plates and shells can generally be idealised by distinct stages (Figure 1). Stage I is described by a linear elastic material behaviour and an uncracked cross-section, Stage II corresponds to linear elastic material behaviour considering a cracked cross-section, and Stage III represents the ultimate strength. Upon cracking of an element, the neutral axis shifts towards the compressed face, causing an extension of the element in its mid-plane. As this extension is generally restrained by surrounding elements, it generates CMA.

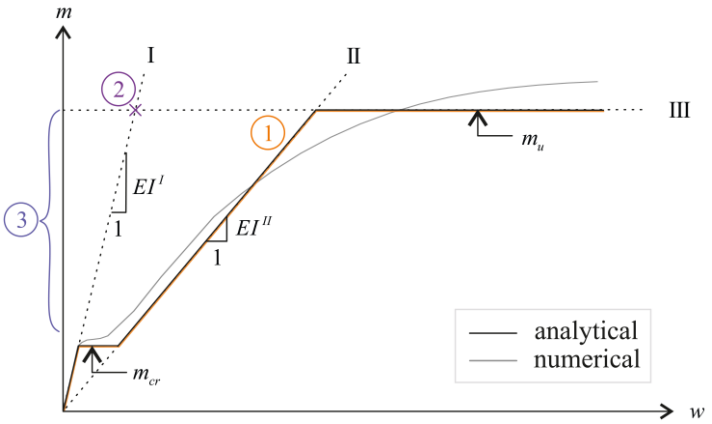

Figure 1: Schematic diagram showing the load-deformation behaviour of RC analytically and numerically (1): Total load-deformation path; (2): ULS, elastic – plastic (EP), (3): SLS or FLS, elastic – elastic (EE)

Analysing the structural response of plates and shells using these three stages (Figure 1: Scenario 1, orange) is intricate, particularly due to the discontinuities, and neglects effects such as tension stiffening or compression softening of the concrete. Instead, nonlinear finite element analyses (NLFEA) are thus often carried out to achieve sufficiently accurate results [2,3] capturing all relevant influences. Such realistic analyses are particularly important for the accurate quantification of CMA, where a precise description of the deformation state [4] is paramount. Analytical solutions for the load-deformation relationship only exist for special cases (e.g. pure twisting moments [5] or anticlastic bending [6]).

In the ultimate limit state (ULS), RC plates and shells can readily be designed based on the theory of plasticity (Figure 1: Stage III). According to the lower bound theorem of plasticity theory, structural safety is ensured by providing sufficient resistance against any statically admissible stress state, see e.g [1]. Using linear elastic FEA, an admissible stress state of any shell and plate can easily be determined (Figure 1: Scenario 2, purple), and the resistances may be determined using well-established yield conditions. The normal moment yield condition [7], also known as Wood-Armer moments, is typically applied for slabs with vanishing membrane forces. Similarly, the sandwich model [9] can be used for shell structures. Because the deformations calculated using linear elastic FEA (Stage I) are smaller than the effective deformations, CMA (if membrane forces are part of the analysis at all) and the ultimate load are underestimated [10]. As the internal actions are determined elastically, but the yield conditions used are based on plasticity theory, the approach outlined above for the ULS design of shells and plates is referred to as elastic-plastic analysis (EP) in the following.

When designing RC shells and plates in the serviceability limit state (SLS) or fatigue limit state (FLS), the focus lies on calculating crack widths or steel stresses, respectively. These values need to be determined considering cracked-elastic cross-sections in Stage II (Figure 1: Scenario 3, blue). In the

following, this approach is termed elastic-elastic analysis (EE). Such analyses are currently only possible in general cases with NLFEA; mechanically consistent analytical models to determine the steel stresses or crack widths in RC plates or shells for SLS or FLS have not been published to the authors' knowledge, except for the mentioned special cases [5,6].

As the SLS and FLS for shells and plates are becoming increasingly important in designing new or examining existing RC structures, simpler and effective methods for the reliable and efficient design and assessment in the SLS and FLS are thus desirable. As a first step to this end, this study highlights open questions and gaps in the state of the art in a case study of a shell predominantly loaded by twisting moments. A restraint factor is introduced to account for CMA in a mechanically consistent manner. Finally, ways in which the identified open questions about the mechanical behaviour of concrete shells and plates might be tackled are presented to allow for more efficient RC shell designs in the future.

2. Case Study

To illustrate the research gaps, analyses of the full load-deformation behaviour, as well as the two design scenarios (EP, EE), are conducted. As a case study, a shell element of a RC bridge deck subjected to predominant twisting moments (Figure 2) is chosen, and the results are compared to the results of a test series carried out by Marti, Leesti and Khalifa [11], who subjected square RC plates with dimensions of 1.70·1.70·0.20 m^3 to pure twisting moments by corner forces. Note that as common in RC analysis and design, normal and twisting moments are referred to the orthogonal reinforcement directions *x* and *y*.

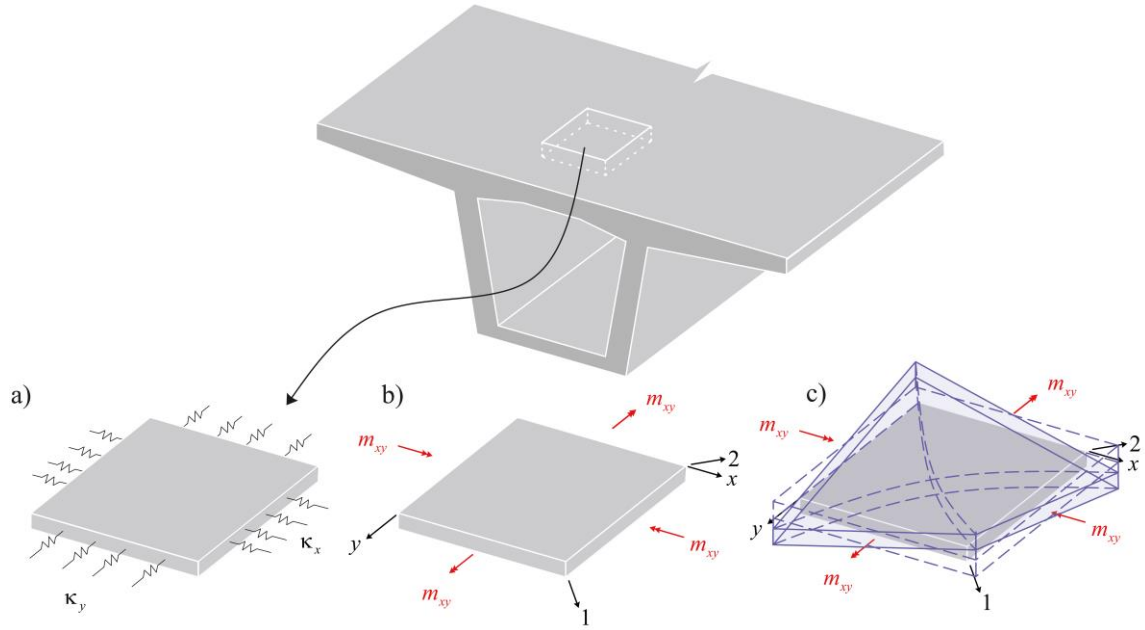

Figure 2: Shell element in the context of a bridge deck: a) in-plane restraint, b) stress state, c) displacements

The experiment evaluated is the – with the exception of the reinforcement layer offsets – isotropically reinforced Specimen ML9. The corresponding material parameters are listed in Table 1. The same calculations are also carried out for Specimen ML8 (orthotropically reinforced), see Appendix A.

Table 1: Material and geometrical parameters for the test specimen ML9 analysed in this case study [11]

Material Parameters		ML9	
Young's modulus steel	E_s	205	GPa
Yield strength steel	f_{sy}	412	MPa
Ultimate strength steel	f_{su}	600[(1)]	MPa
Ultimate strain steel	ε_{su}	100[(1)]	‰
Young's modulus concrete	E_c	35.4	GPa
Compressive strength concrete	f_{cc}	44.4	MPa

Geometrical Parameters		ML9	
Plate thickness	h	200	mm
Plate side widths	s	1700	mm
Static depth	d_x	166	mm
	d_y	182	mm
Reinforcement ratios (a_s/h)	ρ_x	1.00	%
	ρ_y	1.00	%

[(1)] assumptions based on the reinforcing steel designation in [11]

2.1 Load-deformation behaviour

To determine the load-deformation behaviour, a NLFE analysis was carried out using the cracked membrane material model [4] designed explicitly for RC loaded in plane stress, which was implemented as a user material in Ansys Mechanical APDL (CMM-Usermat) [12] to allow for analyses of RC shell structures with the layered Shell181 element of Ansys [12]. A bilinear approximation of the bare steel stress-strain relationship and a concrete stress-strain relationship according to Sargin [13] are applied. For more details on the modelling assumptions, such as the underlying bond-slip relationship or tension stiffening and test recalculations, the reader is referred to [2,3].

Figure 3a) shows the finite element model and the applied boundary conditions. After applying the dead load, the shell is loaded by imposed deformations δ_Q until the ultimate twisting moment of $m_{xy} \approx 85\ kNm/m$ is reached. To account for possible CMA (not present in the experiments), Link180 elements [14] with finite element stiffness $k_{f,x} = k_{f,y} = k_f$ are introduced as shown in Figure 3b). Varying the stiffness k_f allows investigating the influence of CMA ($n_x \neq 0, n_y \neq 0$ and $n_{xy} = 0$) on the laod-deformation behaviour of the shell.

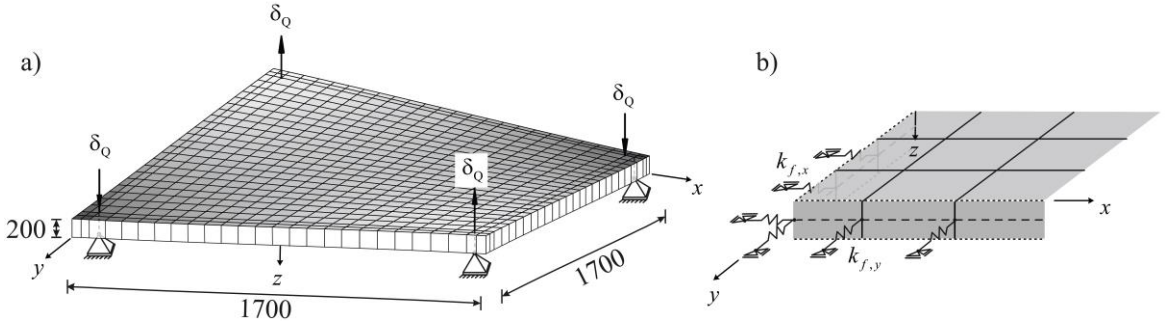

Figure 3: Numerical modelling of the shell element in Ansys: a) FE model, b) Link180 elements in FE model

2.2 Ultimate limit state (EP)

In ULS design, the lower bound theorem of plasticity theory can be applied. Accordingly, a lower limit value of the ultimate load is obtained if a statically admissible stress state is found that does not infringe the yield condition. For vanishing membrane forces ($n_x \approx 0, n_y \approx 0,\ n_{xy} \approx 0$) as in the experiment, the normal moment yield condition [7] can be used, i.e., for pure twisting ($m_x = m_y = 0$):

$$m_{xu} \geq m_x + k|m_{xy}| = k|m_{xy}| \tag{1}$$

$$m_{yu} \geq m_y + \frac{1}{k}|m_{xy}| = \frac{1}{k}|m_{xy}| \tag{2}$$

where m_{xu} and m_{yu} are the required ultimate moments in x- and y-direction, m_x, m_y and m_{xy} the acting moments and k a freely selectable parameter, reasonably set to $k = 1$ for isotropically reinforced specimen ML9. For significant membrane forces ($n_x \neq 0, n_y \neq 0,\ n_{xy} \approx 0$, tension positive), the sandwich model [9] is used as a yield condition to determine the ultimate twisting moment:

$$|m_{xy}| \leq m_{xu} - z \cdot \frac{n_x}{2}, \quad \text{but} \quad |m_{xy}| \leq k_c f_{cc} \frac{h^2}{8} \tag{3}$$

$$|m_{xy}| \leq m_{yu} - z \cdot \frac{n_y}{2}, \quad \text{but} \quad |m_{xy}| \leq k_c f_{cc} \frac{h^2}{8} \tag{4}$$

where z denotes the inner lever arm, and k_c represents the effectiveness factor, reducing the concrete compressive strength for plastic analysis. The upper bound of the torsional resistance (right terms in equations (3) and (4), respectively), was introduced by Nielsen [7] and represents a concrete crushing failure mode instead of the desired ductile failure mode due to the yielding of all reinforcements.

The normal moment yield condition (1, 2) and the sandwich model (3, 4) lead to approximately the same solution for vanishing membrane and shear forcses and an isotropically reinforced RC shell element. Both yield conditions assume a rigid plastic stress-strain relationship for the reinforcing steel and an

arbitrary stress-strain relationship for the concrete. Furthermore, the ductility conditions, e.g. reinforcement yielding, must be fulfilled. In this study, the inner lever arm of forces z_{NMYC} and z_{SM} for the normal moment yield condition and sandwich model, respectively, as well as the ultimate moments m_{xu} and m_{yu} are determined neglecting the compressive reinforcement, i.e.:

$$z_{NMYC} = d - \frac{a_s \cdot f_s}{2 \cdot f_{cc}} \tag{5}$$

$$z_{SM} = h/2 \tag{6}$$

$$m_{xu} = a_{sx} \cdot f_{sx} \cdot z \text{ and } m_{yu} = a_{sy} \cdot f_{sy} \cdot z \tag{7}$$

where d refers to the static depth of the bottom reinforcement and a_s is the reinforcement area. The lever arm of the sandwich model is defined as $h/2$ here due to the state of pure twisting moment.

2.3 Serviceability Limit State Fatigue (EE)

As outlined in the introduction, no analytical solution exists for the calculation of stresses in the reinforcement for an EE analysis under general loading. Therefore, although it is not applicable for this case, the normal moment yield condition (1, 2) is often used in practice, to determine the reinforcement stresses from the resulting bending moments $m_{Ex} = m_x + k|m_{xy}|$ and $m_{Ey} = m_y + 1/k\,|m_{xy}|$ by modelling the shell as two one-dimensional beams in x- and y-direction each. Assuming a cracked cross-section (Stage II) and linear elastic behaviour, the following equations hold:

$$\sigma_s = \frac{m_E}{bd} \frac{1}{\rho\left(1 - \frac{\xi}{3}\right) + \rho'\left(\frac{\xi}{3} - \frac{d'}{d}\right)\left(\frac{\xi - d'/d}{1 - \xi}\right)} \tag{8}$$

$$\frac{x}{d} = \xi = \sqrt{[n\rho + \rho'(n-1)]^2 + 2\left[n\rho + \frac{d'}{d}\rho'(n-1)\right]} - [n\rho + \rho'(n-1)] \tag{9}$$

where x is the compression zone depth, b the width of the cross-section, σ_s the stress in the reinforcement, $n = E_s/E_c$ the modular ratio (where E_s, E_c are the Young's moduli of reinforcement and concrete), and $\rho = a_s/d$ and $\rho' = a_s'/d$ denote the reinforcement ratios of the top and bottom reinforcement, respectively.

Marti and Kong [5] published a mechanically consistent analytical solution to determine the steel stresses in the cracked elastic Stage II for vanishing membrane forces and the special load condition of pure twisting moments and symmetrical (top and bottom identical) iso- or orthotropic reinforcement. In this study, their solution is amended by introducing a restraint factor κ allowing to analytically incorporate membrane forces ($n_x \neq 0, n_y \neq 0,\ n_{xy} \approx 0$):

$$\kappa_x = -\frac{n_x}{\varepsilon_{0x} E_c h};\ \kappa_y = -\frac{n_y}{\varepsilon_{0y} E_c h} \tag{10}$$

where ε_{0x} and ε_{0y} denote the mean strain in the mid-plane of the shell element in the *x* and *y* direction, respectively. A value of $\kappa = 0$ corresponds to an unrestrained shell without CMA. On the other hand, $\kappa = 1$ accounts for a fully restrained system, i.e. $n_x = \varepsilon_{0x} E_c h$ and $n_y = \varepsilon_{0y} E_c h$.

Figure 4 illustrates the behaviour for an isotropically reinforced element, hence $\kappa_x = \kappa_y = \kappa$. By considering equilibrium, a factor α_κ (depth of neutral axes in principal directions) can be determined analogously to the definition of α_{MK} by Marti und Kong [5], but extended for normal membrane forces. Consequently, the torsional stiffness of the shell $D_{xy}(\kappa)$ and reinforcement stresses $\sigma_s(\kappa)$ as well as the mean concrete compressive stresses $\sigma_c(\kappa)$, are obtained as functions of the restraint factor κ :

$$-F_c + 2 \cdot F_s = -n_x \tag{11}$$

$$-\frac{E_c}{2} \cdot \chi_{xy} h^2 \left(\frac{1}{2} - \alpha\right)^2 + 2 \cdot \chi_{xy} \alpha h a_s n E_c = -\kappa \chi_{xy} \alpha h E_c h$$

$$\text{simplifies to:} \quad \frac{\alpha^2}{2} + \frac{1}{8} - \frac{\alpha}{2} - 2n\rho\alpha - \kappa\alpha = 0$$

$$\alpha_{MK} = \frac{1}{2} + 2n\rho - \sqrt{2n\rho(1+2n\rho)} \tag{12}$$

$$\alpha_{\kappa} = \frac{1}{2} + (2n\rho+\kappa) - \sqrt{(2n\rho+\kappa)(2n\rho+\kappa+1)} \tag{13}$$

$$D_{xy}(\kappa) = \frac{m_{xy}}{\chi_{xy}} = \frac{E_c h^3}{24}(4\alpha_{\kappa}^3 - 3\alpha_{\kappa} + 1) \tag{14}$$

$$\sigma_s(\kappa) = E_s \alpha_{\kappa} h \cdot \frac{m_{xy}}{D_{xy}} \tag{15}$$

$$\sigma_c(\kappa) = \sigma_s(\kappa) \cdot \frac{\kappa}{n} \tag{16}$$

The torsional stiffness D_{xy} (14), the steel stresses σ_s (15), and the mean concrete compressive stress σ_c (16) are readily obtained as functions of the restraint factor κ for any given valid twisting moment. Note that the mean concrete compressive stresses $\sigma_c(\kappa)$, corresponding to an uncracked homogeneous cross-section subjected to the resulting strain in the mid-plane, are a measure of the activated CMA.

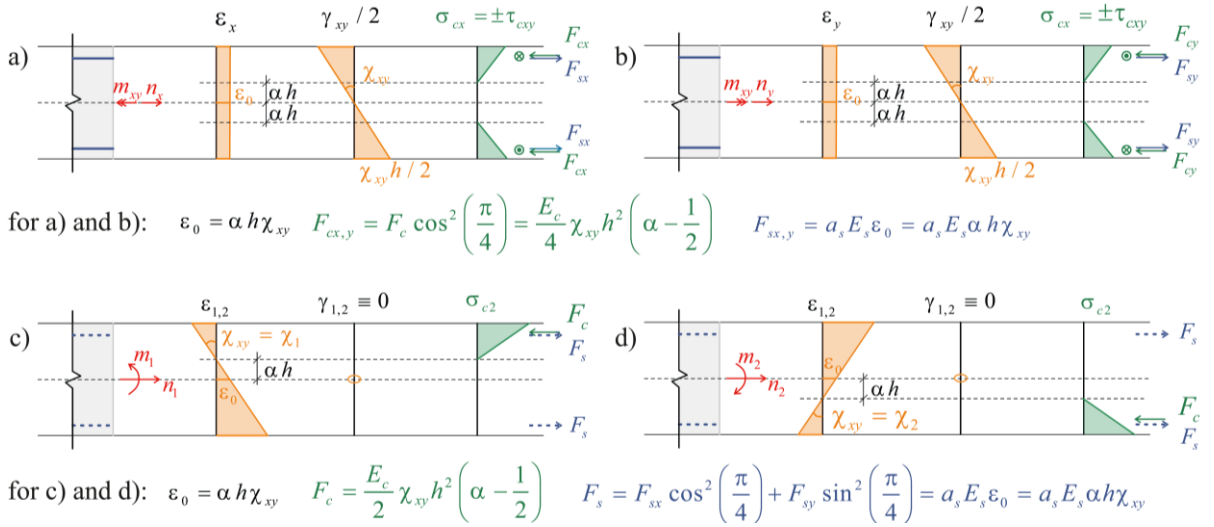

Figure 4: Cross-sections of shell element subjected to pure twisting moment with strains (orange), stresses (green) and forces (blue): a) reinforcement direction *x*, b) reinforcement direction *y*, c) principal direction 1, d) principal direction 2

3. Results and Discussion

This section compares and discusses the results of the load-deformation analysis and the two design scenarios (EP, EE). The results of the anisotropically reinforced Specimen ML8 are compiled in Appendix B.2 (Table 5, Table 6, Figure 8 and Figure 9). In general, the results extracted from the NLFE analysis (generalised stresses m_{xy}, n_x and n_y and generalised strains $\varepsilon_{0x}, \varepsilon_{0y}$ and χ_{xy}) are mean values along the the axis of symmetry of the shell, where the twisting moment m_{xy} is approximately constant (see Appendix B.1, Figure 7). The steel stresses at the crack σ_{srx} and σ_{sry} are also mean values along the axes of symmetry, determined as average stresses in the top and bottom reinforcement in the corresponding directions and accounting for the influence of the bending moments due to dead load. The remaining quantities (mean concrete compression stress σ_c and torsional moment stiffness D_{xy}) are derived from these mean values.

3.1 Load-deformation behaviour

Figure 5a) compares the observed load-deformation behaviour of Specimen ML9 to the NLFEA solutions for different stiffnesses k_f. Triangles in Figure 5a) represent the ultimate twisting moments m_{xyu} based on the normal moment yield condition and the sandwich model according to Section 3.2. Additionally, the onset of yielding in the first reinforcement layer is marked with an "x". The numerical simulation for $k_f = 0$ fits well to the experimental results, confirming that the numerical model reliably

predicts the load-deformation behaviour. As expected, the shell stiffness in Stage II and the ultimate load both increase with the stiffness k_f. The reported failure mode of test specimen ML9 was concrete softening or crushing due to increasing transverse strains $\varepsilon_1 \geq 0$ [5]. The predicted failure mode correlates with this observation, which corresponds to the softening behaviour of the load-deformation curve after the maximum twisting moment. With increasing stiffness k_f, this failure mode becomes more pronounced as the mean concrete compressive stresses σ_c (hence CMA) also increase significantly (Figure 5b)). After stabilised cracking at $m_{xy} \approx 30$ kNm/m, the restraint factor κ decreases with increasing twisting moment m_{xy} and decreasing torsional stiffness D_{xy}, as illustrated by Figure 5c) and Figure 5d) respectively. The decreasing torsional stiffness D_{xy} in Stage II is caused by the progressive reduction of the compression zone depths (which are not constant as in the analytical model). After yielding of the reinforcement (Stage III), the torsional stiffness decreases even more pronouncedly, see Figure 5d).

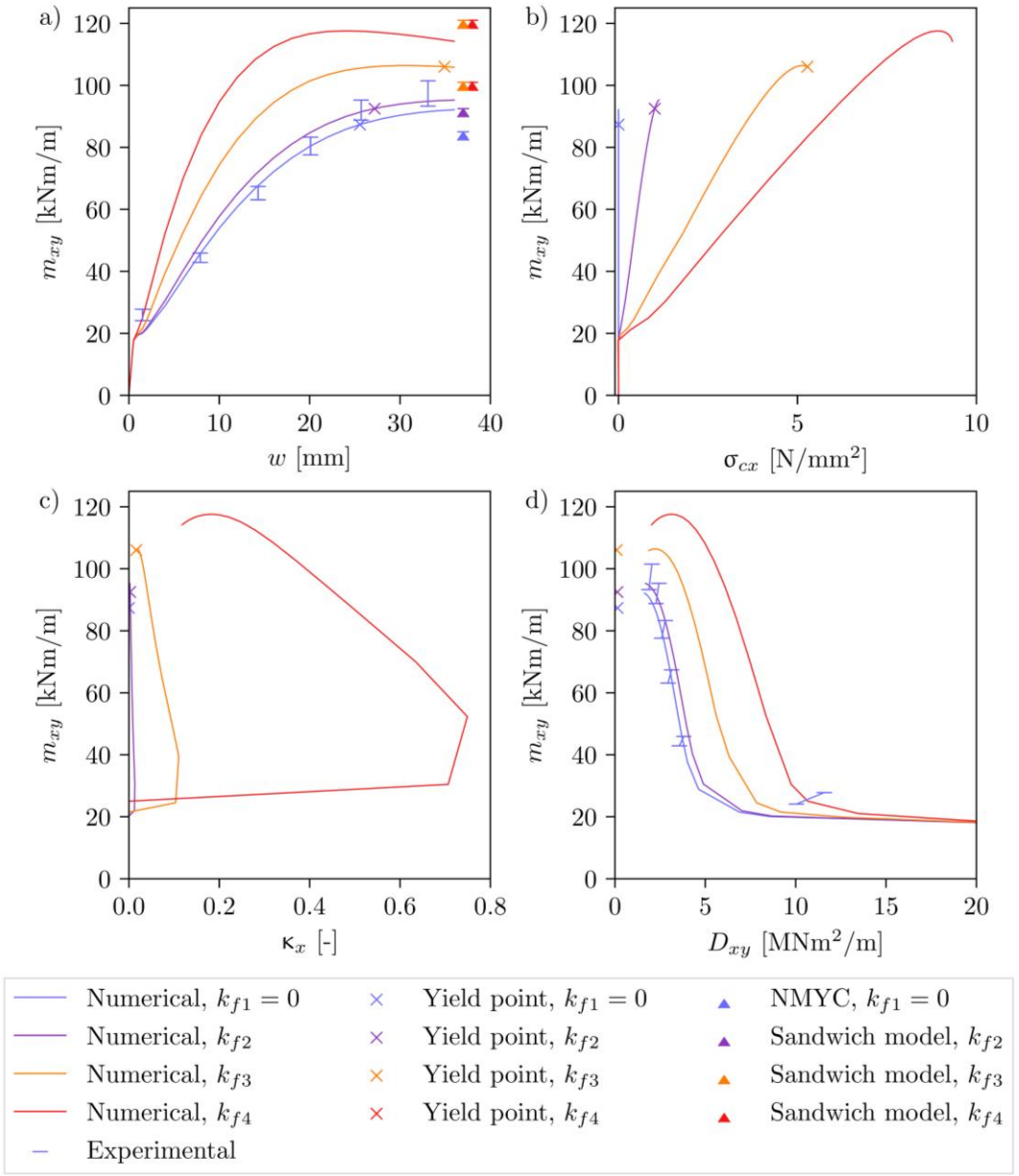

Figure 5: NLFEA results ML9: a) load-deformation behaviour, b) mean compressive stress σ_{cx}, c) restraint factor κ_x, and d) stiffness D_{xy} (corresponding to $k_{f,1..4} = [0, 13, 120, 1'100]$ kN/m; $n_{1..4}$ see Table 2). *Note:* Here, D_{xy} is the secant stiffness, determined from corner deflections w assuming homogeneous m_{xy} and χ_{xy}: $D_{xy} = m_{xy}/\chi_{xy} = m_{xy}l^2/(4w)$

Appendix B.1 (Figure 7) provides more in-depth information about the distribution of m_{xy} and the remaining stress resultants, including the mean transverse shear force v_0, enabling a comprehensive understanding of the force flow within the shell allowing for generalisation of previous findings.

3.2 Ultimate Limit State (EP)

The results of the EP analysis are listed in Table 2. For $n_i = 0$ and $\kappa = 0$ the ultimate twisting moment is calculated with the normal moment yield condition. For $k_f \neq 0$, hence $n_i \neq 0$, the ultimate twisting moment is calculated with the sandwich model and the value of n_i obtained from the NLFE analysis.

Table 2: Ultimate twisting moments according to EP analysis methods

Theory	σ_c [N/mm²]	n_i [kN/m]	m_{xyu} $(k = 1)$ [kNm/m]
Normal moment yield condition	0	0	85
Sandwich model	0	0	82
Sandwich model	-1.01	-202	92.5
Sandwich model	-5.28	-1056	$101^{(1)}/121^{(2)}$
Sandwich model	-8.94	-1788	$101^{(1)}/121^{(2)}$

$0.46^{(1)} \leq k_c \leq 0.55^{(2)}$

All results are based on the material parameters summarised in Table 1 and agree very well with the experimental ultimate load and the NLFE analysis (see also Figure 5). For higher mean concrete compressive stresses $\sigma_c = \sigma_{cx} = \sigma_{cy}$ failure occurs due to concrete softening or crushing. To ensure a safe design, it is advised to choose k_c carefully, as it directly affects the ultimate twisting moment m_{xyu}. The values in Table 2 (see footnote) are chosen according to the SIA 262 [15] for varying f_{cc}.

3.3 Serviceability and Fatigue Limit State (EE)

For a SLS or FLS verification, stresses in the reinforcement in Stage II need to be calculated. This section presents the results for Specimen ML9 according to the normal moment yield condition (Table 3), the analytical evaluation and the NLFE analysis at an acting twisting moment of $m_{xy} = 70\ kNm/m$ in Stage II.

Table 3: Results of the stress calculation for tests ML9 according to the normal moment yield condition

		ML9, k = 1.0	ML9, k = 1.1
Stresses in the bottom reinforcement	$\sigma_{s,x}$	159 MPa	170 MPa
	$\sigma_{s,y}$	198 MPa	170 MPa
Stresses in the top reinforcement	$\sigma'_{s,x}$	58 MPa	62 MPa
	$\sigma'_{s,y}$	38 MPa	33 MPa
Stresses in concrete	σ_c	14 MPa	15 MPa

While the normal moment yield condition is often used in practice, several underlying assumptions are mechanically inconsistent for its application in Stage II (see Section 2.3). To highlight these inconsistencies ands the effect of CMA, Figure 6 compares the results of (i) the analytical method including the restraint factor κ, evaluated for different reinforcement ratios $\rho = 0.2 \ldots 2\%$, (ii) the NLFE analysis of Specimen ML9 ($\rho = 1\%$), and (iii) the normal moment yield condition (Table 3, $k = 1.1$).

Regarding the effect of CMA, both Figure 6a) and b) – and both the analytical model as well as the NLFE analysis – highlight that already at very small restraint (low values of restraint factor κ), the stresses in the reinforcement decrease significantly compared to the case of pure twisting without CMA: For example, a restraint factor of $\kappa = 0.2$ is sufficient at a reinforcement ratio of $\rho = 0.2\%$ to reduce the reinforcement stresses by more than 80%. For larger reinforcement ratios ρ, the beneficial effect of CMA is less pronounced, but still considerable. The reinforcement stresses obtained from the normal moment yield condition are unconservative at low restraint, but progressively become very conservative with increasing κ. CMA thus has a highly beneficial effect, which should be leveraged to design more

materially efficient RC structures and reduce strengthening or replacing existing RC structures due to structural deficiencies (which are often presumed based on analyses neglecting CMA).

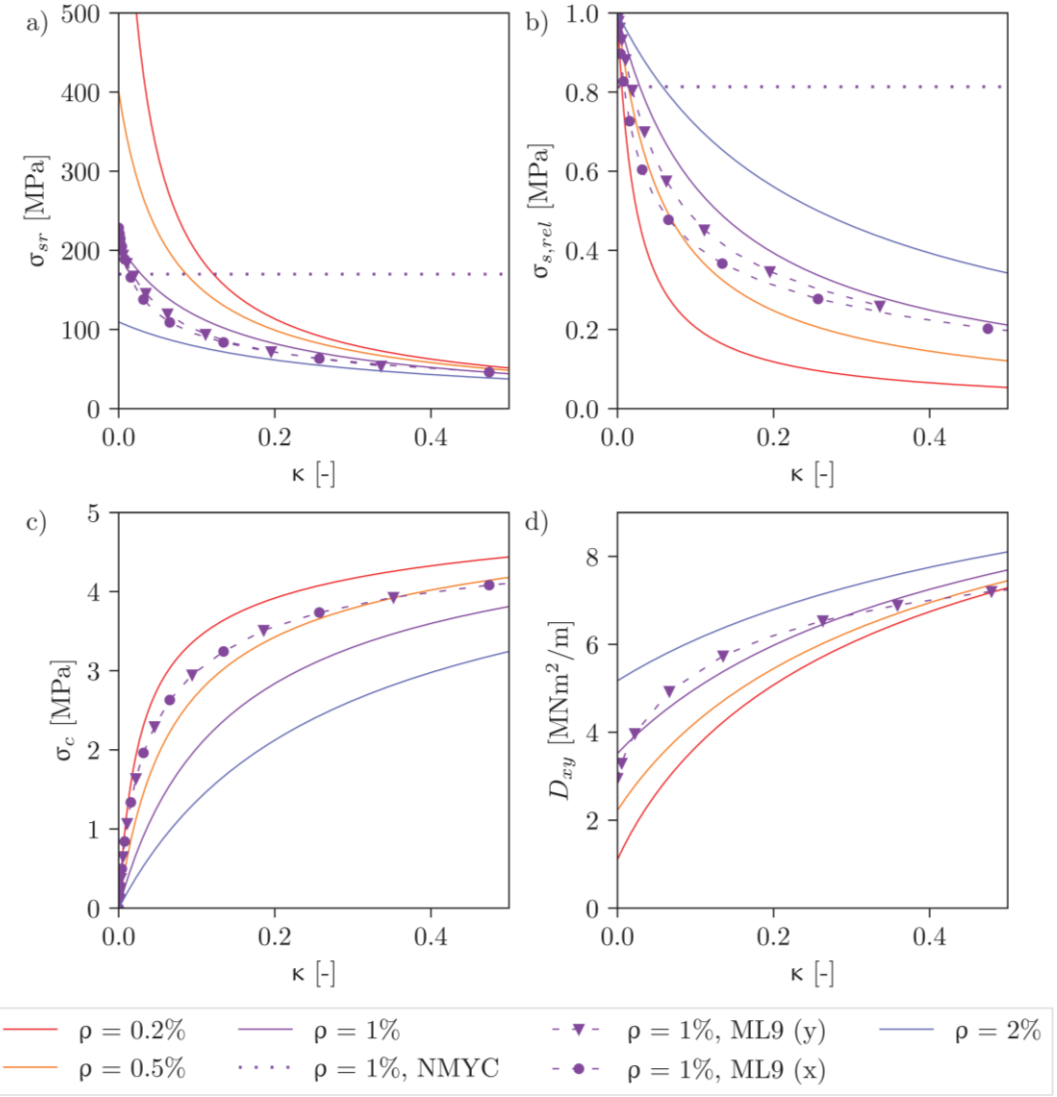

Figure 6: Results of (i) the analytical calculation including κ for different reinforcement ratios ρ (continuous lines), (ii) the NLFE analysis for the reinforcement ratio $\rho = 1\%$ as present in specimen ML9 (dashed lines), and (iii) the normal moment yield condition calculation (dotted lines) for: a) reinforcement stress, b) relative reinforcement stress (normalised with stress at $\kappa = 0$), c) mean concrete compressive stress, and d) stiffness

The analytical method correlates well with the NLFE analysis, hence also the experimental investigation, with differences caused e.g. by the nonlinear material model used in the NLFEA, which also considers tension stiffening and the concrete tensile strength ($f_{ct} = 0.3 f_{cc}^{2/3}$) until cracking of each layer [16], as well as further differences between the NLFE model and the analytical approach (see Section 3). While the differences are minor, it must be noted that the restraint factor κ is a priori unknown, i.e., the application of the analytical model relies on an assumption which highly affects the outcomes but can currently only be determined with NLFE analyses. To yield realistic predictions of CMA, NLFEA must therefore accurately account for the complex mechanical behaviour of RC shell elements, including cracking, tension stiffening and compression softening, even though they are generally sensitive to the boundary conditions. Remarkably, experimental data for the calibration of NLFEA is extremely scarce.

Figure 6c) shows the mean concrete compressive stresses, highlighting that they (hence CMA) are much less sensitive to the restraint factor κ than the reinforcement stresses σ_{sr}. On the other hand, the torsional stiffness D_{xy} increases significantly with κ, see Figure 6d), which is relevant e.g. for deflections of RC structures or soil-structure interaction.

4. Conclusions and Outlook

This paper highlights that the behaviour of RC shells is no solved problem: Even though a safe design in ULS is straightforward based on the lower bound theorem of plasticity theory, obtaining realistic predictions of the load-deformation behaviour or the reinforcement stresses in SLS and FLS requires computationally very expensive NLFE analyses. No analytical models, nor sufficient experimental data to calibrate NLFE analyses are available for plate elements subjected to general loading, even in the simple case without CMA. By assuming proportionality of CMA to the mid-plane strains of a shell element, this study enhances a previously proposed analytical model for shell elements subjected to pure twisting moments by the effect of CMA. The parametric study with this model, as well as the NLFE analyses, highlight that the response is highly sensitive to CMA, with the latter being highly beneficial for reinforcement stresses. This should be be leveraged in the design and assessment of RC structures.

More research is thus required to improve existing methods in the analysis of RC shells by developing efficient tools for realistic analyses of plate and shell structures, particularly regarding the reliable quantification of CMA. NLFE models must be experimentally validated for general loading including CMA, and should be augmented by emerging machine learning-based FEA techniques. Finally, simplified approaches for use in practice must be developed to allow for a widespread adaptation.

References

[1] Marti P. Theory of Structures: Fundamentals, Framed Structures, Plates and Shells. 1st ed. Berlin, Germany: Ernst & Sohn; 2013.
[2] Thoma K. Finite element analysis of experimentally tested RC and PC beams using the cracked membrane model. Eng Struct 2018;167:592–607. https://doi.org/10.1016/j.engstruct.2018.04.010.
[3] Thoma K, Roos P, Weber M. Finite-Elemente-Analyse von Stahlbetonbauteilen im ebenen Spannungszustand: Scheiben- und Plattenberechnungen auf der Grundlage des gerissenen Scheibenmodells. Beton- Stahlbetonbau 2014;109:275–83. https://doi.org/10.1002/best.201300087.
[4] Kaufmann W, Marti P. Structural Concrete: Cracked Membrane Model. Journal of Structural Engineering 1998;124. https://doi.org/10.1061/(ASCE)0733-9445(1998)124:12(1467).
[5] Marti P, Kong K. Response of Reinforced Concrete Slab Elements to Torsion. J Struct Eng 1987;113:976–93. https://doi.org/10.1061/(ASCE)0733-9445(1987)113:5(976).
[6] Marti P, Kaufmann W, Seelhofer H, Karagiannis D. Kirchhoff–Love Plate Deformations Reinterpreted. J Eng Mech 2022;148:04022026. https://doi.org/10.1061/(ASCE)EM.1943-7889.0002105.
[7] Nielsen MP. On the strength of reinforced concrete discs. vol. no. 70. Copenhagen: The Danish Academy of Technical Sciences; 1971.
[8] Kaufmann W. Advanced Structural Concrete, Lecture Notes, Chapter 5: Slabs 2023.
[9] Marti P. Design of Concrete Slabs for Transverse Shear. ACI Struct J 1990;87:180–90. https://doi.org/10.14359/3137.
[10] Thoma K, Malisia F. Compressive membrane action in RC one-way slabs. Eng Struct 2018;171:395–404. https://doi.org/10.1016/j.engstruct.2018.05.051.
[11] Marti P, Leesti P, Khalifa WU. Torsion Tests on Reinforced Concrete Slab Elements. J Struct Eng 1987;113:994–1010. https://doi.org/10.1061/(ASCE)0733-9445(1987)113:5(994).
[12] Thompson MK, Thompson JM. ANSYS Mechanical APDL for Finite Element Analysis. Butterworth-Heinemann; 2017.
[13] Sargin M. Stress-Strain Relationships for Concrete and the Analysis of Structural Concrete Sections. Study Solid Mech Div Univ Waterloo 1971.
[14] Thompson MK, Thompson JM. Chapter 5 - Defining Material Properties. In: Thompson MK, Thompson JM, editors. ANSYS Mech. APDL Finite Elem. Anal., Butterworth-Heinemann; 2017, p. 147–61. https://doi.org/10.1016/B978-0-12-812981-4.00005-8.
[15] SIA 262. Betonbau; 2013.
[16] Raphael JM. Tensile Strength of Concrete. J Proc 1984;81:158–65. https://doi.org/10.14359/10653.

Appendix

A. Methodology

Table 4 states the material parameters of the test specimen ML8.

Table 4: Material parameters for the test specimen ML8 [11]

Material Parameters		ML8	
Young's modulus steel	E_s	205	GPa
Yield strength steel x	f_{sy}	412	MPa
y		479	MPa
Ultimate strength steel	f_{su}	600(1)	MPa
Ultimate strain steel	ε_{su}	100(1)	‰
Young's modulus concrete	E_c	35.41	GPa
Compressive strength concrete	f_{cc}	49.1	MPa

Geometrical Parameters		ML8	
Plate thickness	h	200	mm
Plate side widths	s	1700	mm
Static depth	d_x	168	mm
	d_y	182	mm
Reinforcement ratios (a_s/h)	ρ_x	1.00	%
	ρ_y	0.25	%

(1) assumptions based on the reinforcing steel designation in [11]

B. Results

B.1 Additional results for specimen ML9

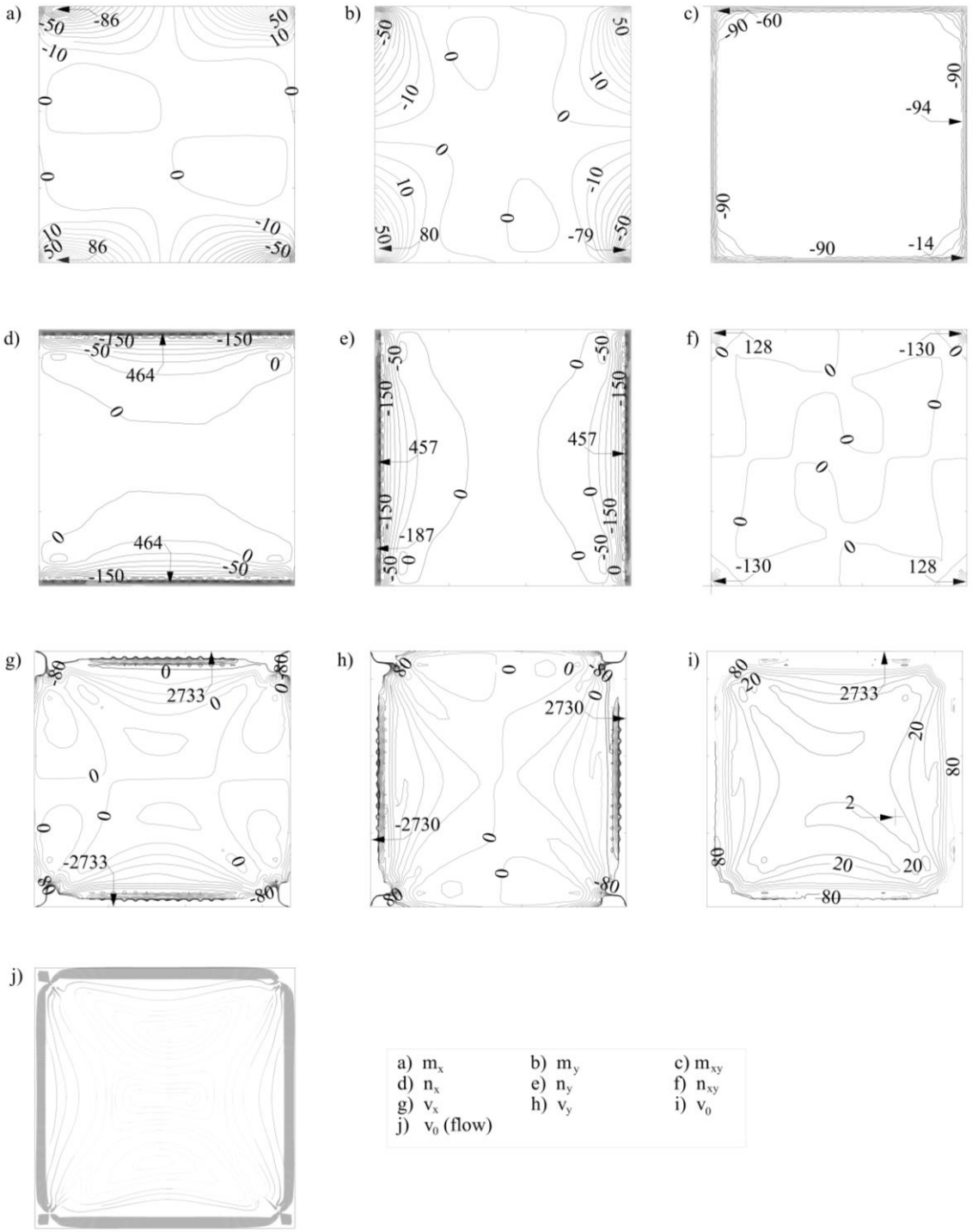

Figure 7: Detailed results of the stress state in test specimen ML9

B.2 Results for specimen ML8

The results of Specimen ML8 are structured analogously to Specimen ML9: Figure 8 shows the load-deformation behaviour of ML8 and Table 5 provides the results of the EP analysis.

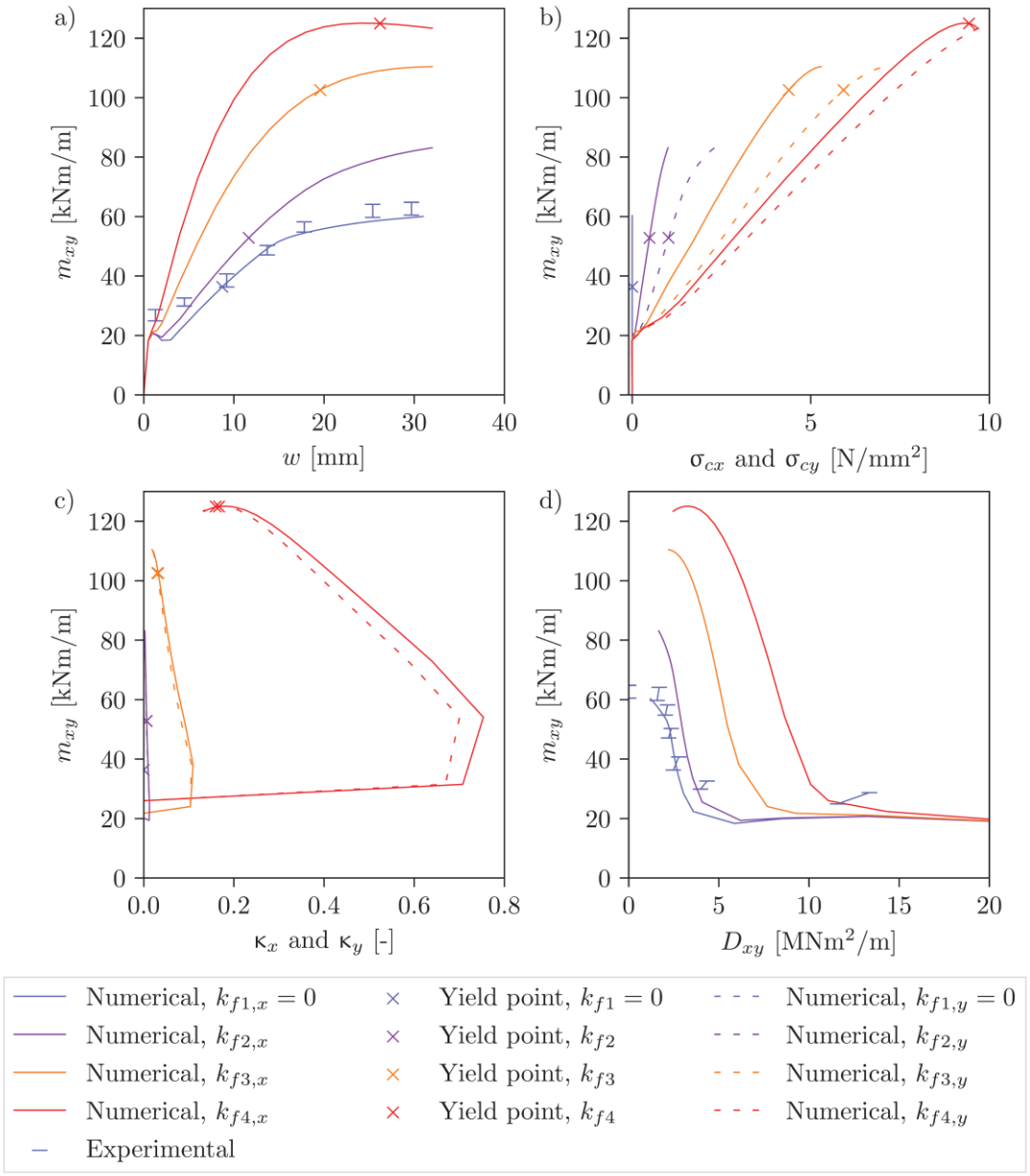

Figure 8: NLFEA results ML8: a) load-deformation behaviour, b) mean compressive stress σ_c, c) restraint factor κ, and d) stiffness D_{xy} (corresponding to $k_{f,1..4} = [0, 13, 120, 1'100]$ kN/m; $n_{1..4}$ see Table 5). *Note:* Here, D_{xy} is the secant stiffness, determined from corner deflections w assuming homogeneous m_{xy} and χ_{xy}:
$D_{xy} = m_{xy}/\chi_{xy} = m_{xy}l^2/(4w)$

Table 5: Ultimate twisting moments according to EP analysis methods for Specimen ML8

Theory		σ_c [N/mm²]	n_i [kN/m]	m_{xyu} $(k = 1)$ [kNm/m]
Normal moment yield condition	x	0	0	152
	y	0	0	37
Sandwich model	x	0	0	96
	y	0	0	21
Sandwich model	x	-0.48	-96	101
	y	-1.02	-204	31
Sandwich model	x	-4.38	-876	$112^{(1)}/135^{(2)}$
	y	-5.92	-1184	80
Sandwich model	x	-9.43	-1886	$112^{(1)}/135^{(2)}$
	y	-10.40	-2080	$112^{(1)}/135^{(2)}$

$0.46^{(1)} \leq k_c \leq 0.55^{(2)}$

Table 6 summarises the stresses in the reinforcement and concrete according to the approximation with the NMYC for an EE analysis, and Figure 9 shows the numerical simulation for ML8 including the previous diagrams of ML9 for comparison.

Table 6: Results of the stress calculation for tests ML8 according to the NMYC

		ML8
Stresses in the bottom reinforcement	$\sigma_{s,x}$	159 MPa
	$\sigma_{s,y}$	908 MPa
Stresses in the top reinforcement	$\sigma'_{s,x}$	58 MPa
	$\sigma'_{s,y}$	-26 MPa
Stresses in concrete	σ_c	14 MPa

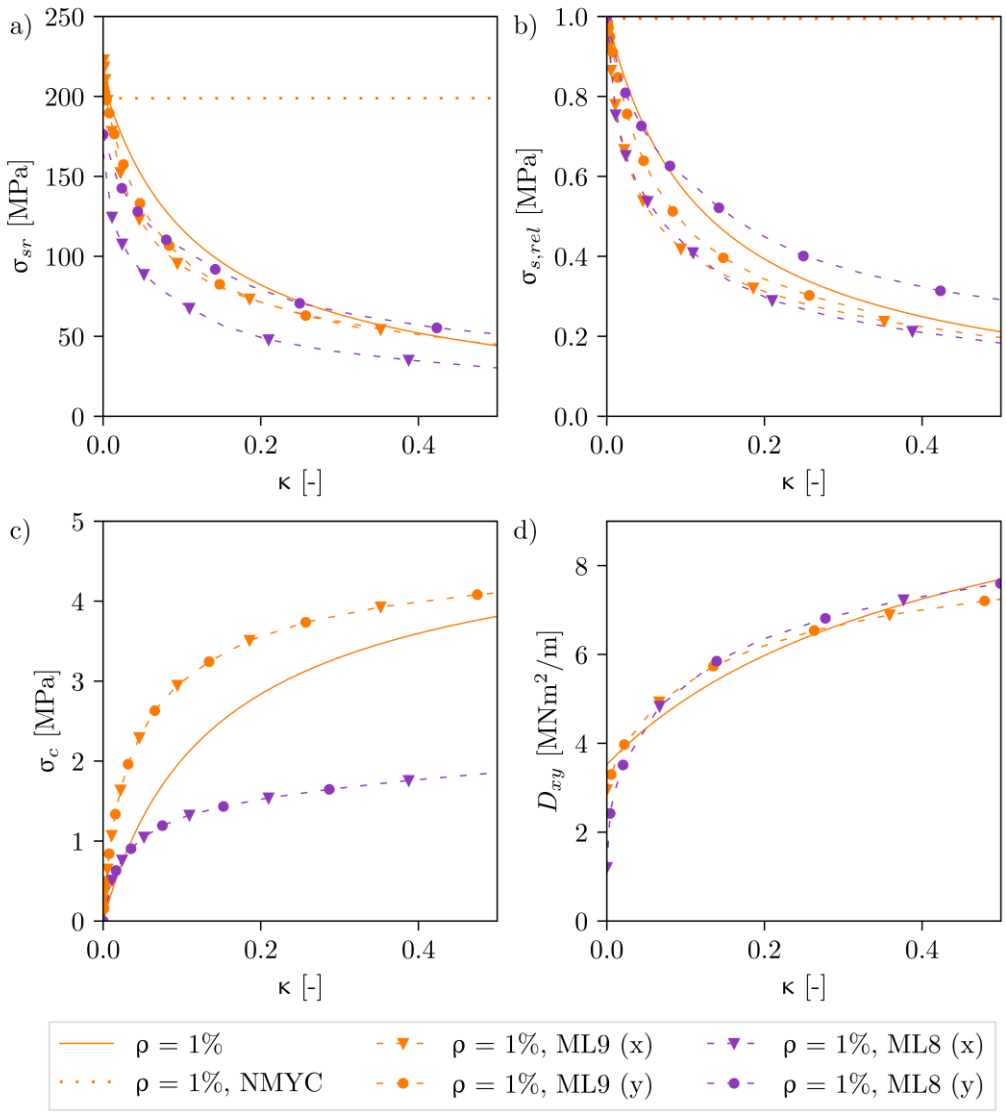

Figure 9: Results of (i) the analytical calculation including κ for different reinforcement ratios ρ (continuous lines), (ii) the numerical simulation for the reinforcement ratio $\rho = 1\%$ present in specimens ML8 and ML9 (dashed lines), and (iii) the normal moment yield condition calculation (dotted lines) for: a) Steel stress, b) Relative steel stress, c) Concrete stress, d) Stiffness

C. List of Symbols

a_s, a_s'	Top and bottom reinforcement area
$\alpha_{MK}, \alpha_\kappa$	Parameter indicating position of neutral axes in principal directions of the analytical model, in the original case of Marti-Kong (MK) or the amended case with restraint factor κ)
b	Cross-section width (in plates: b = 1m)
γ_{xy}	Shear strains
D_{xy}	Torsional stiffness of plate or shell
d_x	Static depht (*x*-direction)
d_y	Static depth (*y*-direction)
δ_Q	Imposed deformations
E_c	Young's modulus of concrete
E_s	Young's modulus of steel
EI^I, EI^{II}	Stiffness in Stages I (uncracked elastic) and II (cracked elastic) (see Figure 1)
ε_1	Transverse strains
ε_{su}	Ultimate strain of steel
$\varepsilon_{0x}, \varepsilon_{0y}$	Mean strain in the midplane of the shell element in *x*-and *y*-direction
F_c	Concrete force
F_s	Steel force
f_{cc}	Compressive strength of concrete
f_{ct}	Tensile strength of concrete
f_{su}	Ultimate strength of steel
f_{sy}	Yield strength of steel
h	Plate thickness
k	Factor that may be chosen freely
k_c	Concrete compressive strength reduction factor for plastic analysis
$k_{f,x}, k_{f,x}$	Finite element stiffness in *x*- and *y*-direction
κ_x, κ_y	Restraint factor in *x*- and *y*-direction
m_{xy}	Twisting moment
m_x, m_y, m_1, m_2	Bending moments in *x*- and *y*-direction or principal directions 1 and 2
m_{xu}, m_{yu}	Ultimate bending moment in *x*- and *y*-direction
m_{xyu}	Ultimate twisting moment
n	$= \frac{E_s}{E_c} =$ modular ratio, i.e. ratio of Young's moduli of concrete and steel

$n_x, n_y, n_{xy}, n_1, n_2$	Normal membrane forces in *x*- and *y*-direction or principal directions 1 and 2
ρ_x, ρ_y	Reinforcement ratio (*x*- and *y*-direction)
s	Plate side lengths
σ_c	Concrete stresses
σ_{sx}, σ_{sy}, $\sigma'_{sx}, \sigma_{sy}{}'$	Reinforcement stresses in *x*- and *y*-direction in top and bottom reinforcement
$\sigma_{s,rel}$	$= \sigma_s(n_i)/\sigma_s(n = 0)$ Relative stresses in the reinforcement (compared to the stresses without any CMA)
σ_{sr}	Steel stresses at the crack
τ_{xy}	Shear stresses
v_0	Mean shear stress
v_x, v_y	Shear forces in *x*- and *y*-direction
w	Deformation
x	Compression zone height or coordinate axis
ξ	$= x/d$ relative depth of compression zone
χ, χ_{xy}	Curvature, twist
y	Coordinate axis
z	Inner lever arm or coordinate (out-of-plane)
z_{SM}, z_{NMYC}	Inner lever arm (for sandwich model and normal moment yield condition)